IJMMM International Journal of Minerals, Metallurgy and Materials 矿物冶金与材料学报（英文版）

Preparation and oxidation characteristics of $ZrC–ZrB_2$ composite powders with different proportions

Yu Wang, Guohua Zhang, and Kuochih Chou

Cite this article as:
Yu Wang, Guohua Zhang, and Kuochih Chou, Preparation and oxidation characteristics of $ZrC–ZrB_2$ composite powders with different proportions, *Int. J. Miner. Metall. Mater.*, 29(2022), No. 3, pp. 521-528. https://doi.org/10.1007/s12613-021-2330-2

View the article online at SpringerLink or IJMMM Webpage.

Articles you may be interested in

Yu Wang, Guo-hua Zhang, Yue-dong Wu, and Xin-bo He, Preparation of CaB_6 powder via calciothermic reduction of boron carbide, *Int. J. Miner. Metall. Mater.*, 27(2020), No. 1, pp. 37-45. https://doi.org/10.1007/s12613-019-1873-y

Yuan Gao, Zong-de Liu, Qi Wang, and Yong-tian Wang, Microstructure and mechanical properties of $Nb–Mo–ZrB_2$ composites prepared by hot-pressing sintering, *Int. J. Miner. Metall. Mater.*, 25(2018), No. 7, pp. 824-831. https://doi.org/10.1007/s12613-018-1631-6

Yu Wang, Yue-dong Wu, Ke-han Wu, Shu-qiang Jiao, Kuo-chih Chou, and Guo-hua Zhang, Effect of NaCl on synthesis of ZrB_2 by a borothermal reduction reaction of ZrO_2, *Int. J. Miner. Metall. Mater.*, 26(2019), No. 7, pp. 831-838. https://doi.org/10.1007/s12613-019-1794-9

Song Chen and De-gui Zhu, Influence of sintering temperature on the phases and photoelectric characteristics of BiOCl/ZnO composite powders, *Int. J. Miner. Metall. Mater.*, 24(2017), No. 12, pp. 1438-1447. https://doi.org/10.1007/s12613-017-1537-8

Yang Sun, Yong Li, Li-xin Zhang, Shi-ming Li, Ming-wei Yan, and Jia-lin Sun, Novelty phase synthesis mechanism and morphology in resin-bonded $Al-Al_2O_3-TiO_2$ composites at high temperatures under flowing N_2, *Int. J. Miner. Metall. Mater.*, 26(2019), No. 9, pp. 1177-1185. https://doi.org/10.1007/s12613-019-1829-2

Ya-ran Zhang, Qi Cai, Yong-chang Liu, Zong-qing Ma, Chong Li, and Hui-jun Li, Evaluation of precipitation hardening in TiC-reinforced Ti_2AlNb-based alloys, *Int. J. Miner. Metall. Mater.*, 25(2018), No. 4, pp. 453-458. https://doi.org/10.1007/s12613-018-1591-x

IJMMM WeChat

QQ author group

International Journal of Minerals, Metallurgy and Materials
Volume 29, Number 3, March 2022, Page 521
https://doi.org/10.1007/s12613-021-2330-2

Preparation and oxidation characteristics of ZrC–ZrB_2 composite powders with different proportions

Yu Wang, Guohua Zhang✉, *and Kuochih Chou*

State Key Laboratory of Advanced Metallurgy, University of Science and Technology Beijing, Beijing 100083, China
(Received: 28 April 2021; revised: 15 June 2021; accepted: 11 July 2021)

Abstract: ZrC and ZrB_2 are both typical ultra-high temperature ceramics, which can be used in the hyperthermal environment. In this study, a method for preparing ultrafine ZrC–ZrB_2 composite powder was provided, by using the raw materials of nano ZrO_2, carbon black, B_4C, and metallic Ca. It is worth pointing out that ZrC–ZrB_2 composite powder with any proportion of ZrC to ZrB_2 could be synthesized by this method. Firstly, a mixture of ZrC and C was prepared by carbothermal reduction of ZrO_2. By adjusting the addition amount of B_4C, ZrC was boronized by B_4C to generate ZrC–ZrB_2 composite powder with different compositions. Using this method, five composite powders with different molar ratios of ZrC and ZrB_2 (100ZrC, 75ZrC–25ZrB_2, 50ZrC–50ZrB_2, 25ZrC–75ZrB_2, and 100ZrB_2) were prepared. When the temperature of boronization and decarburization process was 1473 K, the particle size of product was only tens of nanometres. Finally, the oxidation characteristics of different composite powders were investigated through oxidation experiments. The oxidation resistance of ZrC–ZrB_2 composite powder continued to increase as the content of ZrB_2 increased.

Keywords: borides; carbides; core-shell structures; powders; ultra-high temperature ceramic

1. Introduction

ZrC and ZrB_2 are all classified as ultra-high temperature ceramic due to their high melting points of above 3273 K [1]. Both ZrC and ZrB_2 contain strong covalent bonds, but they belong to different crystal system (Fig. 1(a) and (b)). The lattice of ZrC is cubic system and has a wide range of stoichiometry, wherein C/Zr molar ratio varies from 0.56 to 1.0 [2]. ZrB_2 belongs to hexagonal system and has a poor damage tolerance because of its covalent bond and narrow range of stoichiometry [3]. In addition, the physical parameters of ZrC and ZrB_2 are also different. The specific parameters are shown in Table 1 [4]. It was concluded that they can coexist in a large temperature range [5].

Compared with single-phase ceramics, ZrC–ZrB_2 composite ceramics have more advantages. The microstructure can be optimized through compounding with another phases. In boride-based composites, ZrC will inhibit abnormal grain growth [6]. Meanwhile, the physical properties of the composite material can be adjusted particularly simply by changing the composition. Eutectic alloys were found to reveal minimal wear, maximal friction, maximal bending, and compressive strengths and minimal hardness when compared to no eutectic ZrB_2–ZrC compositions [5]. Li *et al*. [7] showed that the addition of ZrC can improve the plasticity of ZrB_2. Asl *et al*. [8] pointed out that higher fraction of *in-situ* synthesized ZrC is an important toughening phase for ZrB_2-based ceramics. In addition, it was indicated in many investigations that ZrB_2–SiC–ZrC (ZSZ) ternary composite materials have excellent comprehensive performances [9–11]. Owing to the excellent performances, the potential uses of ZrC–ZrB_2 composite ceramics include heat shielding materials [12–14], cutting tools [10,15–17], wear-resistant coatings [18–21], brazing fillers [22–23], etc.

Due to the excellent performances of ZrC–ZrB_2 based composite ceramics, many methods have been reported to synthesize ZrC–ZrB_2 composite powder. Li *et al*. [7] fabricated ZrB_2–ZrC composite nanofibers by electrospinning and carbothermal reduction. Bai *et al*. [24] obtained ultra-fine ZrB_2–ZrC composite powders by radiofrequency thermal plasma synthesis. Chen *et al*. [25] reported the preparation of ZrC–ZrB_2 nano-composite powder from sol–gel method. Tsuchida and Yamamoto [26] used Zr, B, and C elements to prepare composite powder via self-propagating high-temperature synthesis (SHS). The above methods can produce a variety of ZrC–ZrB_2 composite powders with different microstructures. However, composite powders of different proportions cannot be conveniently prepared using cheap raw materials. It is necessary to develop a method that can prepare ultra-fine ZrC–ZrB_2 composite powders with any proportions for the application of ZrC–ZrB_2-based ceramics.

In our previous work, a method for preparing ultra-fine ZrB_2 powder was proposed [27]. The critical steps of that method are the B_4C and melted Ca was used to boronize and

✉ Corresponding author: Guohua zhang E-mail: ghzhang0914@ustb.edu.cn
© University of Science and Technology Beijing 2021

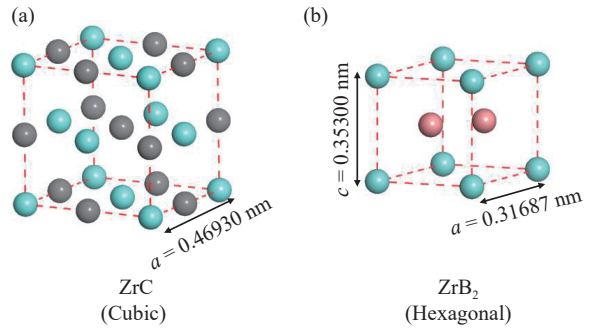

Fig. 1. Lattice model of ZrC (a) and ZrB_2 (b). *a* and *c*: lattice constant.

the carbothermal reduction product of ZrO_2, composed of ZrC and excessive C, was decarburized. Therefore, ZrC–ZrB_2 composite powders with different proportions might be obtained by controlling the addition of B_4C using this method. In this new work, this idea would be verified. Several composite powders with different molar proportions (75ZrC–25ZrB_2, 50ZrC–50ZrB_2, and 75ZrC–25ZrB_2,) were trial-produced. In addition, the oxidation characteristics of composite powders with different components have also been investigated, because the oxidation resistance of ultra-high temperature ceramic materials is an extremely important indicator.

Table 1. Physical parameters of ZrB_2 and ZrC [4]

Compound	Space group	Molar mass / ($g \cdot mol^{-1}$)	Density / ($g \cdot cm^{-3}$)	Vickers hardness / GPa	Elasticity modulus / GPa	Coefficient of thermal expansion / K^{-1}	Thermal conductivity / ($W \cdot m^{-1} \cdot K^{-1}$)	Specific resistance / (10^{-8} Ω·m)
ZrC	Fm-3m	103.23	6.7	20.5 (0.5 N)	495	7.01 (300–1300 K)	27.2 (1770 K) 39.7 (2770 K)	76.5
ZrB_2	P6/mmm	112.84	6.1	22.1 (0.3 N) 17.9 (1 N)	496	5.9 (300–1300 K) 6.5 (1300–2300 K)	23.6 (300 K) 24.1 (473 K)	9.7

2. Thermodynamic analysis

The current method to prepare ZrC–ZrB_2 composite powder includes two high-temperature processes, namely the carbothermal reduction process (reaction (1)) of ZrO_2, as well as the boronization (reaction (2)) and decarburization process (reaction (3)) of ZrC.

$$ZrO_2 + 3C = ZrC + 2CO(g) \quad (1)$$

$$ZrC + 0.5B_4C = ZrB_2 + 1.5C \quad (2)$$

$$Ca + 2C = CaC_2 \quad (3)$$

In order to verify the feasibility of each high-temperature process, the changes of standard Gibbs free energy ($\Delta G^{\ominus}$) of the related reactions were calculated using FactSage7.0 software, as shown in Fig. 2. For carbothermal reduction reaction of ZrO_2, the reaction will proceed spontaneously above 1931 K under standard conditions (p_{CO} = 10^5 Pa). However, under actual condition, vacuum or inert gas flow will lead to a low partial pressure of CO (p_{CO} < 10^5 Pa), which will reduce the critical temperature of carbothermal reaction. From the calculation results, as p_{CO} decreases from 10^5 Pa to 10 Pa, the critical temperature decreases from 1931 to 1331 K. For the boronization and decarburization reactions, the values of their $\Delta G^{\ominus}$ are negative in a large temperature range, and thus the reactions can proceed spontaneously. In summary, the current method for the preparation of ZrC–ZrB_2 composite powder is possible from the viewpoint of thermodynamics.

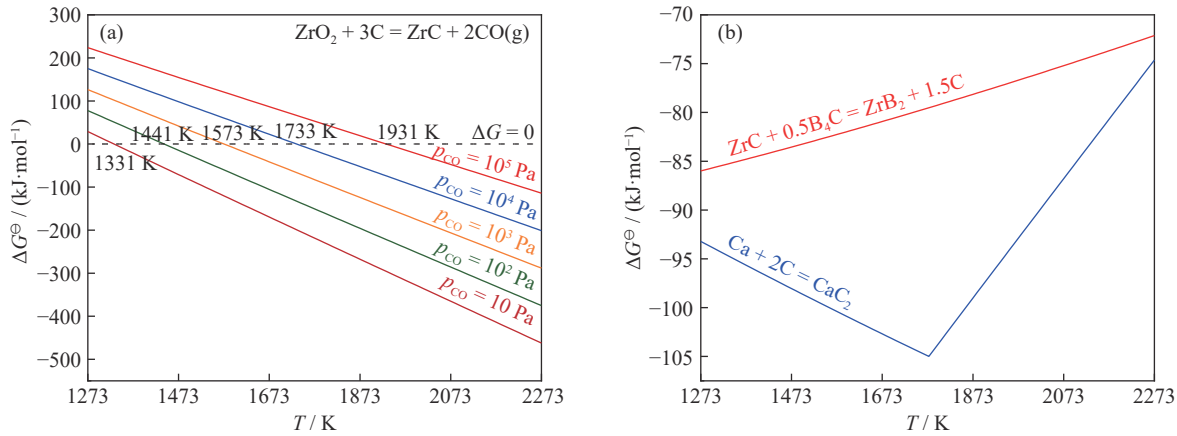

Fig. 2. Changes of the standard Gibbs free energy of related reactions: (a) carbothermal reduction stage; (b) boronization and decarburization stages.

3. Experimental procedures

The raw materials used were nano-ZrO_2 (purity > 99%, Shanghai Macklin Biochemical Co., Ltd., Shanghai, China), carbon black (purity > 98.5%, Mitsubishi Chemical Corporation, Tokyo, Japan), B_4C (purity > 99%, 2–3 μm, Shanghai Aladdin Bio-Chem Technology Co., Ltd., Shanghai, China), and metal calcium (purity > 99.5%, 1–5 mm, Beijing Universal Jin Xin International Science and Technology Co., Ltd., Beijing, China). Field emission scanning electron micro-

scope (FE-SEM) images of raw materials are shown in Fig. 3, from which ZrO_2 and carbon black particles are both nano-sized, while B_4C powder is composed of polyhedral particle with the particle size of several microns. The specific surface area of ZrO_2 and carbon black were characterized by Brunauer-Emmett-Teller (BET) method. The results show that the specific surface areas of ZrO_2 and carbon black are 4.33 and 2.27 $m^2 \cdot g^{-1}$, respectively. After calculation, the equivalent diameters of ZrO_2 and carbon black particles are 47 and 26 nm, respectively.

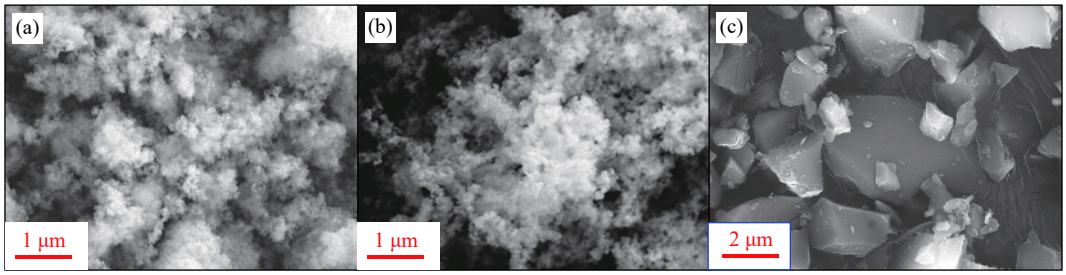

Fig. 3. FE-SEM images of raw materials: (a) nano-ZrO_2; (b) carbon black; (c) B_4C.

In carbothermal reaction stage, powders of nano-ZrO_2 and carbon black with a ZrO_2/C molar ratio of 1:3.6 were homogeneously mixed in agate mortar in a slurry state by adding alcohol. The addition amount of C was higher than theoretical value calculated by the stoichiometric ratio, which was conducive to the reduction of ZrO_2, and meanwhile, the excessive C could also hinder the growth of ZrC particles [28]. After 30 min of manual mixing, the slurry was dried in an oven. Then, the dried mixture was placed and reacted in the electric furnace (with $MoSi_2$ as heating element). The sample was heated with rate of 5 $K \cdot min^{-1}$ in argon gas. According to thermodynamic analysis, to ensure a high reaction rate, the samples were reacted at 1873 K for 4 h. After the furnace was cooled to room temperature, all samples were collected and weighed. In the boronization and decarburization processes, in order to obtain the composite powders with different ratios, according to reaction (2), the ZrC/B_4C molar ratios were 1:0, 1:0.125, 1:0.25, 1:0.375, and 1:0.5, corresponding to the products of 100ZrC, 75ZrC–25ZrB_2, 50ZrC–50ZrB_2, 75ZrC–25ZrB_2, and 100ZrB_2, respectively. Since Ca was easily oxidized and volatile at high temperature, excessive Ca (1.5 times of the theoretical amount) was added to ensure the completion of decarburization reaction (reaction (3)) at 1473 K for 4 h [27–28]. After reaction, the remaining Ca and generated CaC_2 in the product were removed by acidic leaching (HCl, 1 $mol \cdot L^{-1}$). Finally, the products were collected after rinsing and drying.

The phases of the samples were detected using powder X-ray diffraction analysis (XRD, SMARTLAB (9), Cu-K_α radiation, $\lambda = 0.154178$ nm) in a 2θ range of 10°–90° with a scanning rate of 30°·min^{-1}. The morphology of powders was observed using field-emission scanning electron microscope (FE-SEM, GeminiSEM 500) field-emission transmission electron microscopy (FE-TEM, FEI Tecnai G2 F20). The surface area of the samples was determined using the Brunauer-Emmett-Teller method (BET, ASAP-2460, MICROMERITICS, American). The carbon content was determined using a carbon-sulfur analyzer (EMIA-920V2, HORIBA, Japan), and the oxygen content was determined using an oxygen and nitrogen hydrogen analyzer (EMGA-830, HORIBA, Japan). The changes of the Gibbs free energy of reactions were calculated using FactSage 7.0 thermodynamic software. Oxidation characteristics were studied in flowing air using thermal analyser (DTA–TG HENVEN HSC-3).

4. Results and discussion

4.1. Product of carbothermal reduction

The morphology and phase composition of the product prepared after carbothermal reduction reaction are shown in the Fig. 4. There are many fine particles in the area marked by the green circle, and the energy dispersive spectroscopy (ESD) results show that the C content is relatively high in this area. The EDS results of the marked points also show that the characteristic spectral intensity of C with fine particle is significantly higher than that at large particle. It is clearly determined that the fine particles of residual C exist among the sub-micron ZrC particles. The growth of ZrC particles is hindered by the residual C [28]. At the same time, the XRD patterns only show the characteristic peaks of ZrC, while the residual C is not displayed. This result may be due to the low crystallinity of carbon black. According to the above characterization results, it can be known that a mixed powder of ultrafine ZrC and C was prepared via the reaction between nano ZrO_2 and C. The mixture would be used as a raw material for subsequent steps.

4.2. Product of boronization and decarburization process

Fig. 5 displays XRD patterns of the products prepared at 1473 K. Obviously, only the characteristic peaks of ZrC and ZrB_2 are found in all patterns. In addition, with increasing molar fraction of ZrB_2, the peak intensity of corresponding phase became stronger. Furthermore, the corresponding relationship between the composition (mass fraction) of ZrC–ZrB_2 composite powder and the diffraction peak intensity (peak height) was fitted, and the result can be described by Eq. (4).

$$\frac{x_{ZrC}}{x_{ZrB_2}} = 0.542 \frac{I_{ZrC(111)}}{I_{ZrB_2(101)}} \tag{4}$$

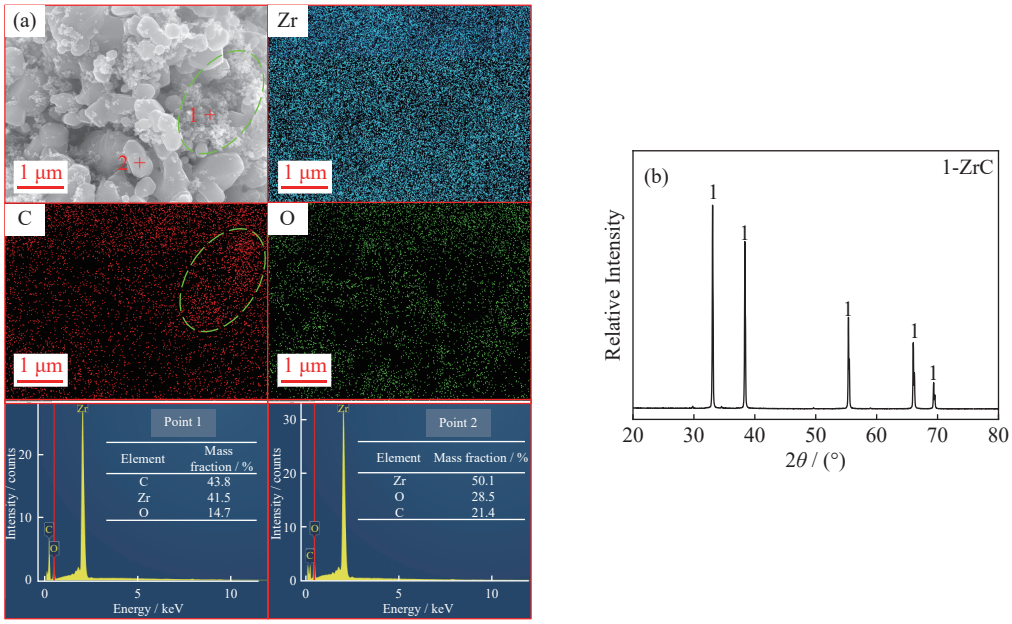

Fig. 4. Morphology and phase of carbothermal reduction product: (a) FE-SEM images and EDS results; (b) XRD patterns.

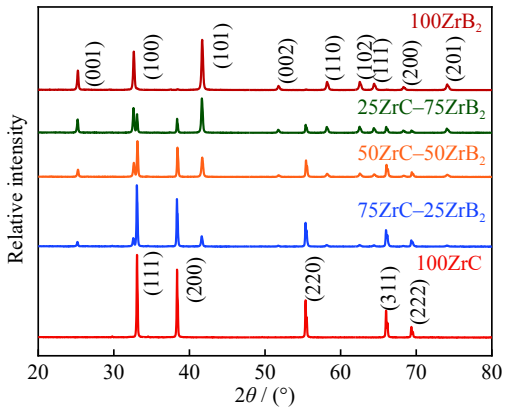

Fig. 5. XRD patterns of the boronization and decarburization products with different proportions obtained at 1473 K for 4 h.

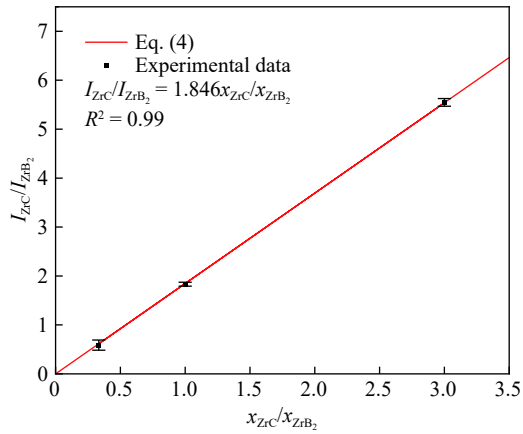

Fig. 6. Fitted curve between mole fraction and peak intensity.

where x_{ZrC} is mole fraction of ZrC; x_{ZrB_2} is mole fraction of ZrB_2; $I_{ZrC(111)}$ is peak intensity of ZrC(111) crystal plane and $I_{ZrB_2(101)}$ is peak intensity of ZrB_2(101) crystal plane. The fitted curve is shown in Fig. 6, and the image shows a linear relationship between molar ratio and peak intensity ratio, with the correlation coefficients of 0.99. This equation can be used to roughly estimate the composition of the composite powder, when the XRD pattern of the powder is gotten.

In addition, the carbon content and oxygen content of different samples are shown in Fig. 7. It is reasonable that the carbon content in the sample shows a downward trend as the ZrC content decreases. However, the oxygen content in the sample has an upward trend with the increase of the ZrB_2 content. In the processes of boronization and decarburization, there should not be so much residual oxygen in ZrC or ZrB_2 particles, due to the excessive addition of Ca. However, the oxidation of ZrB_2 or ZrC particles may occur during the acidic leaching process. There is evidence that ZrB_2 would be more susceptible to corrosion than ZrC under similar acidic conditions [4]. Therefore, as the content of ZrB_2 increases, the acid resistance of sample become worse, and oxygen content in the final sample would also increase.

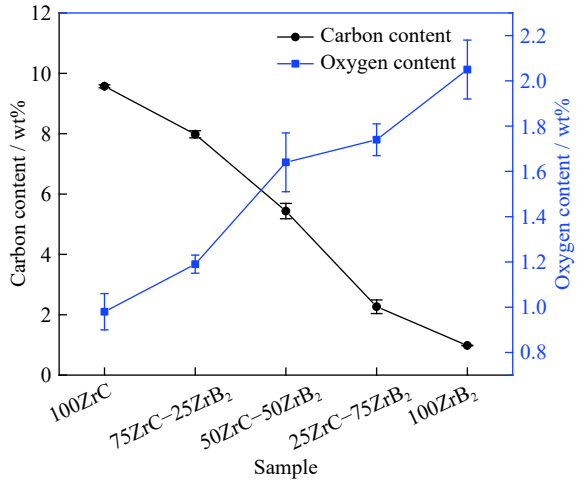

Fig. 7. Carbon and oxygen contents of different samples.

FE-SEM images with high magnifications for different samples have been provided, as shown in Fig. 8. By comparing the morphology of the composite powders with different

proportions, the number of flake shaped particles increases with the increase of ZrB_2 content. However, the two phases could not be identified based on the EDS results. In order to further determine the particle morphology and distribution of different phases, TEM images are provided as shown in Fig. 9. There are two types of shadows (tens of nanometres) in the bright-field image, which are brighter irregular shapes and darker square. According to the mass thickness contrast, it can be analysed that these two shadows correspond to flake particles and cubic particles respectively. Then, the selected area electron diffraction (SAED) and high-resolution transmission electron microscopy (HRTEM) results also indicates that cubic particles are ZrC and flake particles are ZrB_2. In HRTEM image of the ZrC particles, a special core-shell structure with the ZrC particle coated by ZrB_2 layer is observed. Similar structures have also been found in $ZrC–ZrB_2$ composite fibers obtain by carbothermal reduction [7]. The possible reason for this structure is that some ZrC particles are not completely boronized during the boronization process due to the insufficient supply of B_4C. This phenomenon indicates that the boronization process of ZrC particles gradually proceedes from the surface to the core. Through the above analysis, the particle morphology of $ZrC–ZrB_2$ composite powder is identified. The typical morphology of ZrC particles iss cube, and there may be a thin layer of ZrB_2 on the surface of ZrC particles owing to the incomplete boronization reaction. In composite powder, the typical morphology of ZrB_2 is confirmed to be flaky.

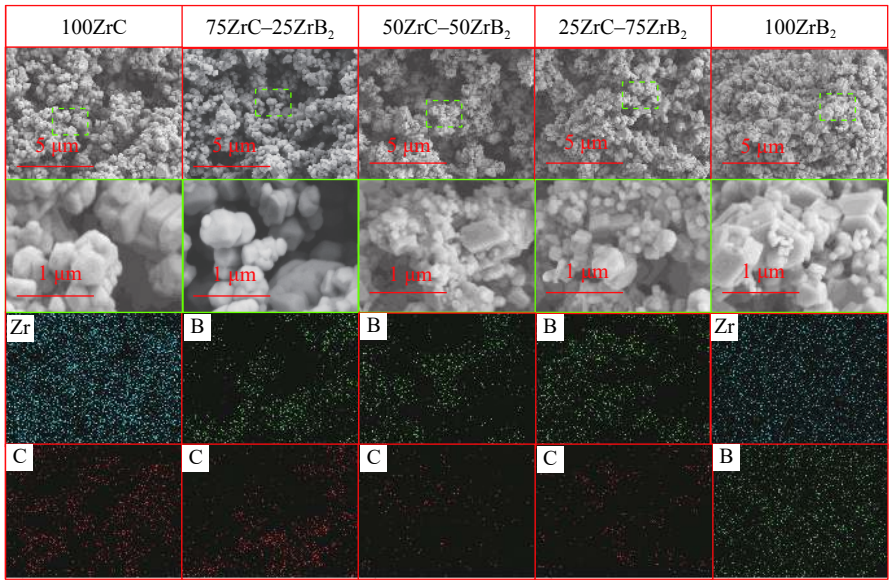

Fig. 8. FE-SEM and EDS images of boronization and decarburization products with different proportions obtained at 1473 K for 4 h. Note: EDS images correspond to high magnification images.

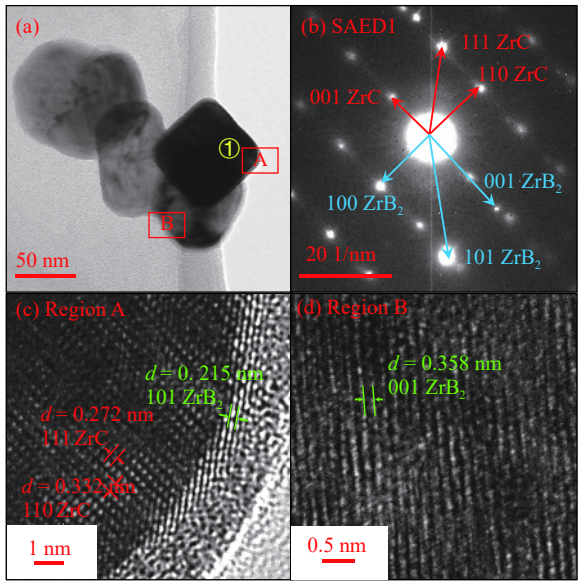

Fig. 9. FE-TEM images of $50ZrC–50ZrB_2$ composite powder obtained at 1473 K for 4 h: (a) bright-field image; (b) SAED pattern; (c, d) HRTEM image.

4.3. Oxidation characteristics of $ZrC–ZrB_2$ composite powder with different proportions

For comparing oxidation characteristics of $ZrC–ZrB_2$ composite powder with different proportions, different samples were heated with a rate of 10 $K \cdot min^{-1}$ in dry air. Fig. 10 displays the TG–DTA curves of oxidation process of $ZrC–ZrB_2$ powders. The oxidation process is divided into several stages according to the TG curve, and the peak temperature of the DTA curve is marked for comparison. The oxidation characteristics of monophase powders (100ZrC and $100ZrB_2$) are the research basis for this study. The oxidation process of the sample 100ZrC is divided into two stages, with two exothermic peaks corresponding to them. In stage Ⅰ, the weight gain is rapid and with a strong exotherm (716 K), which corresponds to reaction (5). In the stage Ⅱ, the weight increases at first and then descends, and a weak exothermic peak is located at 817 K. This stage is the combined effect of weightlessness reaction (reaction (5)) and weight gain reaction (reaction (6)). In order to further confirm the authenticity of reactions (5) and (6), the carbon content of samples at the end of stage Ⅰ and stage Ⅱ were tested,

which were 3.66wt% and 0.02wt%, respectively. Consequently, during the oxidation process of ZrC, C first precipitated from ZrC in low temperature stage, and then is continuously oxidized in high temperature stage. During this process, with the increase of temperature, reaction (5) gradually weakens, and the effect of reaction (6) is gradually revealed. However, different from the case of 100ZrC, the oxidation process of the sample 100ZrB_2 is simple weight gain accompanied by intense exotherm, corresponding to reaction (7). After weight gain process, the TG curve shows a slight weight loss, which is due to the volatilization of B_2O_3 (reaction (8)). The oxidation resistance of ZrB_2 is obviously better than that of ZrC, which is mainly due to the formation of B_2O_3 liquid layer in the oxidation process of ZrB_2 [29]. The liquid layer covers the surface of the particles and hinders the mass transfer of O_2.

$$ZrC + O_2(g) = ZrO_2 + C,\ \Delta H_{273} = -903.569\ kJ \cdot mol^{-1} \quad (5)$$

$$C + O_2(g) = CO_2(g),\ \Delta H_{273} = -393.485\ kJ \cdot mol^{-1} \quad (6)$$

$$ZrB_2 + 2.5O_2(g) = ZrO_2 + B_2O_3,\ \Delta H_{273} = -2049.493\ kJ \cdot mol^{-1} \quad (7)$$

$$B_2O_3 = B_2O_3(g) \quad (8)$$

For the oxidation of sample 75ZrC–25ZrB_2, the whole process is divided into three stages. Compared to oxidation of monophase ZrC, stage Ⅰ corresponds to reaction (5), and the DTA peak position is increased by 42 K, while stage Ⅱ is reaction (6), with the DTA peak position also increases by 31 K. The weight gain in stage Ⅲ corresponds to the oxidation of ZrB_2 (reaction (7)). In the oxidation process of sample 50ZrC–50ZrB_2, the whole process is divided into two parts. Stage Ⅰ corresponds to reactions (5) and (7), and Stage Ⅱ is also the oxidation process of of C. During the rapid weight gain, two strong exothermic peaks are detected, corresponding to reactions (5) and (7), with the peak positions of the two strong exothermic reactions of 886 and 907 K, respectively. Oxidation of C exhibits a weak exothermic peak at 971 K. However, for sample 25ZrC–75ZrB_2 its oxidation behaviour is simple, with only one weight gain process and one exothermic peak (927 K). The oxidation characteristics of ZrC can't be clearly distinguished due to its low content.

By comparing the oxidation characteristics of different samples, as the content of ZrB_2 increases, the oxidation characteristic temperature of ZrC also increases. When the mole fraction of ZrB_2 is greater than 75%, ZrC is protected and oxidized simultaneously with ZrB_2. The hindrance of the B_2O_3

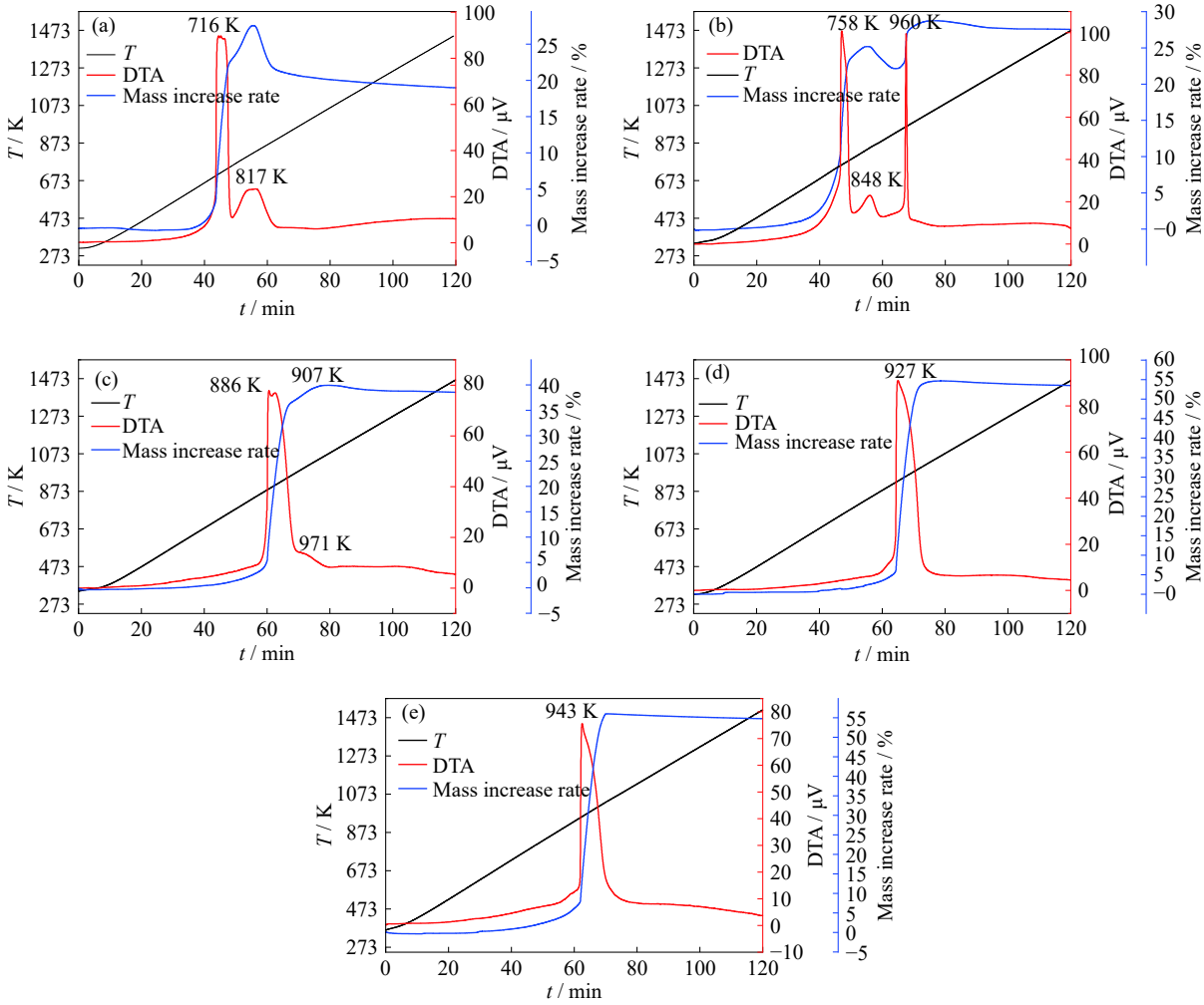

Fig. 10. TG–DTA curves of ZrB_2–ZrC composite powders with different proportions in oxidation process: (a) 100ZrC; (b) 75ZrC–25ZrB_2; (c) 50ZrC–50ZrB_2; (d) 25ZrC–75ZrB_2; (e) 100ZrB_2.

liquid layer to oxygen mass transfer could explain this phenomenon. As the content of ZrB_2 increases, the amount of liquid B_2O_3 produced by initial oxidation increases and evenly coats the particle surface. Especially for ZrC particles, the effective coating of B_2O_3 can make the oxidation of ZrC proceed simultaneously with ZrB_2 (sample 25ZrC–75ZrB_2).

5. Conclusion

In this paper, a two-step method to prepare ZrC–ZrB_2 composite powder with different proportions was proposed. Firstly, a mixture of ZrC and C was prepared by carbothermal reduction of ZrO_2. After that, by controlling the addition amount of B_4C, ZrC was boronized by B_4C to generated ZrC–ZrB_2 composite powder with different compositions. The excessive C was reacted with Ca to form CaC_2 which can be removed by acidic leaching. By this method, five powders with different proportions (100ZrC, 75ZrC–25ZrB_2, 50ZrC–50ZrB_2, 75ZrC–25ZrB_2, and 100ZrB_2) were successfully prepared. According to the microscopic morphology analyses, the particle size of the product prepared at 1473 K was tens of nanometres, among which ZrC and ZrB_2 were cubic and flaky particles, respectively. According to the special core-shell structure, the boronization process of ZrC was inferred that boronization reaction gradually advances from the surface of ZrC particles to core. Finally, the oxidation characteristics of composite powders in different proportions were studied. The test results showed that the oxidation resistance of ZrC–ZrB_2 composite powder continued to increase as the content of ZrB_2 increased. As the mole fraction of ZrB_2 was greater than 75%, the oxidation characteristic of the composite powder was close to that of pure ZrB_2.

Acknowledgement

This work was financially supported by the Fundamental Research Funds for the Central Universities, China (No. FRF-IDRY-19-012).

Conflict of Interest

The authors declare no potential conflict of interest.

References

[1] W.G. Fahrenholtz, E.J. Wuchina, W.E. Lee, and Y.C. Zhou, *Ultra-High Temperature Ceramics: Materials for Extreme Environment Applications*, John Wiley & Sons, Inc., Hoboken, 2014.

[2] C. Nachiappan, L. Rangaraj, C. Divakar, and V. Jayaram, Synthesis and densification of monolithic zirconium carbide by reactive hot pressing, *J. Am. Ceram. Soc.*, 93(2010), No. 5, p. 1341.

[3] D.L.J. Engberg, L. Tengdelius, H. Högberg, M. Thuvander, and L. Hultman, Atom probe tomography field evaporation characteristics and compositional corrections of ZrB_2, *Mater. Charact.*, 156(2019), art. No. 109871.

[4] A.W. Weimer, *Carbide, Nitride and Boride Materials Synthesis and Processing*, Springer, Dordrecht, 1997.

[5] G. Effenberg and S. Ilyenko, *Ternary Alloy Systems*, Springer, Heidelberg, 2009.

[6] F. Adibpur, S.A. Tayebifard, M. Zakeri, and M.S. Asl, Spark plasma sintering of quadruplet ZrB_2–SiC–ZrC–C_f composites, *Ceram. Int.*, 46(2020), No. 1, p. 156.

[7] F.P. Li, Z.L. Xu, K. Zhao, and Y.F. Tang, ZrB_2–ZrC composite nanofibers fabricated by electrospinning and carbothermal reduction: Processing, phase evolution and tensile property, *J. Alloys Compd.*, 771(2019), p. 456.

[8] M.S. Asl, B. Nayebi, S. Parvizi, Z. Ahmadi, N. Parvin, M. Shokouhimehr, and M. Mohammadi, Toughening of ZrB_2-based composites with *in-situ* synthesized ZrC from ZrO_2 and graphite precursors, *J. Sci: Adv. Mater. Devices*, 6(2021), No. 1, p. 42.

[9] D.L. Hu, H. Gu, J. Zou, Q. Zheng, and G.J. Zhang, Core–rim structure, bi-solubility and a hierarchical phase relationship in hot-pressed ZrB_2–SiC–*M*C ceramics (*M* = Nb, Hf, Ta, W), *J. Materiomics*, 7(2021), No. 1, p. 69.

[10] I. Akin and G. Goller, Mechanical and oxidation behavior of spark plasma sintered ZrB_2–ZrC–SiC composites, *J. Ceram. Soc. Jpn.*, 120(2012), No. 1400, p. 143.

[11] A. Rezapour and Z. Balak, Fracture toughness and hardness investigation in ZrB_2–SiC–ZrC composite, *Mater. Chem. Phys.*, 241(2020), art. No. 122284.

[12] Z.L. Xu, K. Zhao, F.P. Li, Y.S. Huo, and Y.F. Tang, The oxidation behavior of ZrB_2–ZrC composite nanofibers fabricated by electrospinning and carbothermal reduction, *Ceram. Int.*, 46(2020), No. 8, p. 10409.

[13] Y. Kubota, M. Yano, R. Inoue, Y. Kogo, and K. Goto, Oxidation behavior of ZrB_2–SiC–ZrC in oxygen-hydrogen torch environment, *J. Eur. Ceram. Soc.*, 38(2018), No. 4, p. 1095.

[14] L. Liu, H.J. Li, W. Feng, X.H. Shi, K.Z. Li, and L.J. Guo, Ablation in different heat fluxes of C/C composites modified by ZrB_2–ZrC and ZrB_2–ZrC–SiC particles, *Corros. Sci.*, 74(2013), p. 159.

[15] L. Xu, C.Z. Huang, H.L. Liu, B. Zou, H.T. Zhu, G.L. Zhao, and J. Wang, *In situ* synthesis of ZrB_2–ZrC_x ceramic tool materials toughened by elongated ZrB_2 grains, *Mater. Des.*, 49(2013), p. 226.

[16] Y. Wang, G.H. Zhang, Y.D. Wu, and X.B. He, Preparation of CaB_6 powder via calciothermic reduction of boron carbide, *Int. J. Miner. Metall. Mater.*, 27(2020), No. 1, p. 37.

[17] Y. Wang, Y.D. Wu, K.H. Wu, S.Q. Jiao, K.C. Chou, and G.H. Zhang, Effect of NaCl on synthesis of ZrB_2 by a borothermal reduction reaction of ZrO_2, *Int. J. Miner. Metall. Mater.*, 26(2019), No. 7, p. 831.

[18] X. Lv, Z.J. Zhan, H.Y. Cao, and C.H. Guo, Microstructure and properties of the laser cladded *in-situ* ZrB_2–ZrC/Cu composite coatings on copper substrate, *Surf. Coat. Technol.*, 396(2020), art. No. 125937.

[19] T.G. Guan, M.Q. Cao, K. Xie, X. Lv, and Y.L. Tan, Microstructure and wear resistance of ZrC–ZrB_2 /Ni composite coatings prepared by plasma transferred arc cladding, *Mater. Res.*, 22(2019), No. 3, art. No. e20180781.

[20] J.X. Hou, J. Fan, H.J. Yang, Z. Wang, and J.W. Qiao, Deformation behavior and plastic instability of boronized $Al_{0.25}$CoCrFeNi high-entropy alloys, *Int. J. Miner. Metall. Mater.*, 27(2020), No. 10, p. 1363.

[21] J.Y. Xu, B.L. Zou, S.M. Zhao, Y. Hui, W.Z. Huang, X. Zhou, Y. Wang, X.L. Cai, and X.Q. Cao, Fabrication and properties of ZrC–ZrB_2/Ni cermet coatings on a magnesium alloy by atmospheric plasma spraying of SHS powders, *Ceram. Int.*, 40(2014), No. 10, p. 15537.

[22] N. Çömez, C. Çivi, and H. Durmuş, Reliability evaluation of hardness test methods of hardfacing coatings with hypoeutectic and hypereutectic microstructures, *Int. J. Miner. Metall. Mater.*, 26(2019), No. 12, p. 1585.

[23] J.D. Jarman, W.G. Fahrenholtz, G.E. Hilmas, J.L. Watts, and D.S. King, Characterization of fusion welded ceramics in the SiC–ZrB_2–ZrC system, *J. Eur. Ceram. Soc.*, 41(2021), No. 4, p. 2255.

[24] L.Y. Bai, F.L. Yuan, Z. Fang, Q. Wang, Y.G. Ouyang, H.C. Jin, J.P. He, W.F. Liu, and Y.L. Wang, RF thermal plasma synthesis of ultrafine ZrB_2–ZrC composite powders, *Nanomaterials*, 10(2020), No. 12, art. No. 2497.

[25] S.G. Chen, Y.Z. Gou, H. Wang, K. Jian, and J. Wang, Preparation and characterization of high-temperature resistant ZrC–ZrB_2 nanocomposite ceramics derived from single-source precursor, *Mater. Des.*, 117(2017), p. 257.

[26] T. Tsuchida and S. Yamamoto, Mechanical activation assisted self-propagating high-temperature synthesis of ZrC and ZrB_2 in air from Zr/B/C powder mixtures, *J. Eur. Ceram. Soc.*, 24(2004), No. 1, p. 45.

[27] Y. Wang, Y.D. Wu, B. Peng, K.H. Wu, and G.H. Zhang, A universal method for the synthesis of refractory metal diborides, *Ceram. Int.*, 47(2021), No. 10, p. 14107.

[28] K.H. Wu, Y. Jiang, S.Q. Jiao, K.C. Chou, and G.H. Zhang, Synthesis of high purity nano-sized transition-metal carbides, *J. Mater. Res. Technol.*, 9(2020), No. 5, p. 11778.

[29] W.M. Guo, G.J. Zhang, Y.M. Kan, and P.L. Wang, Oxidation of ZrB_2 powder in the temperature range of 650–800°C, *J. Alloys Compd.*, 471(2009), No. 1-2, p. 502.